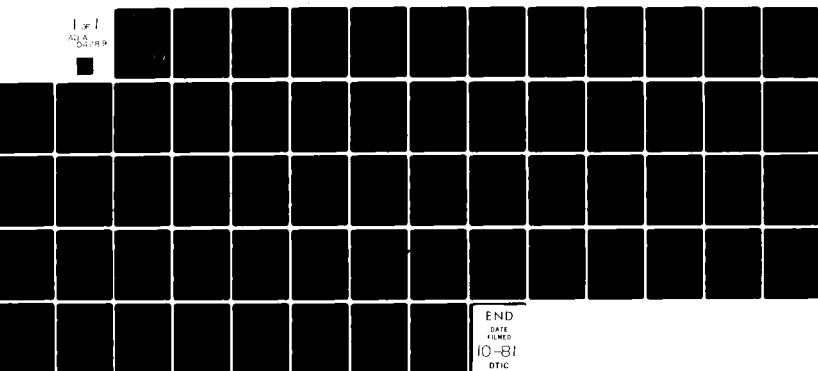


AD-A104 789 CATHOLIC UNIV OF AMERICA WASHINGTON DC VITREOUS STATE LAB F/6 20/6
ELECTRO-OPTICAL WAVEGUIDE DEFLECTORS FOR SIGNAL PROCESSING APPL--ETC(U)
APR 79 C H BULMER N00173-77-C-0245 NL

UNCLASSIFIED

Line 1
AD-A104 789



END
DATE
FILED
10-81
DTIC

LEVEL
ADA104789

APPENDIX
AISL

Report on

Electro-optical Waveguide Deflectors
for Signal Processing Applications

Research performed under Contract N00173-77C-0245 with
the Catholic University of America. (Vitreous State
Laboratory.)

Catherine H. Bulmer

Apr 1979

DTIC
ELECTED
SEP 29 1981
S D
F

DTIC FILE COPY

7-1-51

ELECTRO-OPTICAL WAVEGUIDE DEFLECTORS
FOR SIGNAL PROCESSING APPLICATIONS

This report describes an investigation of the behavior of electro-optical waveguide array deflectors, and of the capabilities and limitations of these integrated optical devices for signal processing applications. The work was performed under Contract N00173-77C-0245 with the Catholic University of America.

Table of Contents

page

Summary	
I Introduction	1
II Analysis of Output Distribution	5
III Deflection Characteristics: Number of Resolvable Spots	9
IV Design Considerations: Near Field Operation and Device Capacitance	16
V Device Performance Characteristics: Bandwidth and Power Related to Number of Spots	23
VI Experimental Comparisons	30
VII Crosstalk	34
VIII Conclusions	38
Acknowledgements	39
Appendix	40
References	41
Figure Captions	43
Figures	

Accession For	
NTIS GRA&I	<input checked="" type="checkbox"/>
DOD TAB	<input type="checkbox"/>
Unannounced	<input type="checkbox"/>
Jurisdiction	<i>ALL C2</i>
By	
Distribution/	
Availability Codes	
Avail and/or	
Dist	Special
A	

SUMMARY

The behavior of various electro-optic waveguide deflectors is analyzed using Fraunhofer diffraction theory to obtain the far field output intensity distributions. In all the devices, a spatially varying phase shift is created electro-optically across the input optical beam. The resulting voltage-dependent optical beam deflection can be continuous or discontinuous. Single prism elements, arrays of identical or phase-staggered prism elements and arrays of channel waveguide elements are described by the same analytic technique. The capacitance of different interdigital electrode structures is determined and is in good agreement with experimental measurements. The capabilities of different deflectors are assessed by comparing number of resolvable spots, power, bandwidth and crosstalk. Comparisons are made with experimental data. Simple phase distributions are demonstrated to be useful for determining most deflection parameters, including the power per unit bandwidth.

I. INTRODUCTION

Optical beam deflection based on the electro-optical effect has long been considered an excellent technique to obtain high speed, high resolution, optical beam steering. With the advent of optical waveguiding techniques, it became apparent that optical beam and electrical field confinement would result in orders of magnitude improved deflection efficiency when compared with deflection implemented with bulk crystals. Signal processing, film processing and communications multiplexing applications based on optical beam deflection have been reexamined in light of the potentially increased performance offered by waveguide deflector geometries and several experimental implementations proposed. However, some early performance projections now appear to be overly optimistic. The purpose of this research was to thoroughly examine the capabilities of waveguide deflector devices and to establish criteria from which realistic predictions of achievable performance might be made.

Electro-optical deflection has been extensively studied in both thin film waveguides and bulk crystals. This deflection is generally accomplished by creating an approximately linear optical phase shift via the electro-optical effect across the width of the input beam. In the simplest case this phase shift may be used to steer the optical beam through refraction. It is desired to accomplish this deflection at high speeds, with little beam distortion and with little crosstalk between the various deflection positions. Ideally, the angle of deflection should increase linearly as the applied voltage is increased. It is found however that the deflected beam motion may be continuous or discontinuous in nature, depending on the geometry of the device employed. Device design thus becomes a critical factor in achieving the desired operating characteristics.

During the course of this work, we examined the principal deflector designs which have been demonstrated or proposed. These designs include single electro-optical prism elements, prism arrays, and arrays of channel waveguides. Deflectors consisting of a single prism element have been demonstrated by Tien⁽¹⁾ and Kaminow⁽²⁾ in planar waveguide form and by Fowler⁽³⁾ in bulk form. These devices possess electrodes positioned at an angle which leads to a gradient in the applied electric field distribution and concomitantly in the induced index profile. Refraction of the input optical beam results. The prism elements can be connected in parallel to form arrays where the waveguide elements are identical, as demonstrated by Tsai,⁽⁴⁾ or non-identical with a staggered phase shift between adjacent elements. The phase-staggered case was demonstrated in bulk form by Ninomiya,⁽⁵⁾ by varying the voltage applied to each element. This design is difficult to realize practically in waveguide form since a different constant phase must be created (such as by using parallel electrodes of varying lengths in front of the prism elements) to add to the identical phase slope of each prism element. Cascaded bulk prism configurations have also been studied by Lee and Zook.⁽⁶⁾ The third type of deflector consists of an array of channel waveguides,^(7,8) in which the electrode lengths are varied in order to impose a different phase shift on the part of the wave propagating in each channel, and hence create an approximately continuous phase slope across the entire wave (an array of such interdigital finger electrodes, with a linear variation in length, can also be formed on a planar waveguide⁽⁹⁾). In bulk form,⁽¹⁰⁾ the same phase front is induced by varying the voltage applied to the channel electrodes which are of constant length.

The various waveguide deflection methods are analyzed in a consistent manner, using Fraunhofer diffraction theory, so that performance comparisons can be made for signal processing applications. The current literature does not permit such evaluation. Specifically, three deflector devices are studied: the single prism, the prism array and the channel waveguide array. The nature of the deflection is determined by classifying the movement of the spot as continuous or discontinuous. The phase change required to produce a certain number of spots is calculated and, for different electrode configurations, the corresponding voltage is found. The capacitance is computed for the various electrode designs in order to compare device speeds. It was found during this analysis that the usual RC bandwidth definition ($\Delta f = (\pi RC)^{-1}$) does not accurately describe the performance of deflectors, particularly in the case of digital deflectors. A new definition of bandwidth was developed and is defined as the speed of the device above which the number of resolvable spots decreases by one. This definition results in the bandwidth becoming a function of the number of spots and is found to be considerably more restricting than the more optimistic RC definition. The number of spots produced for a given power and bandwidth or power/bandwidth ratio are then compared and conclusions are reached as to the capabilities of each device. For the prism array, comparisons are also made with our experimental measurements

of the number of spots, applied voltage and capacitance. We also compare our theoretical predictions with experimental data in the relevant literature, (2,4,7-9) with reasonable agreement.

II. Analysis of Output Distribution

The behavior of different kinds of deflectors can be described by the same analytic technique. The far field output intensity distribution of a deflector is obtained from Fraunhofer diffraction theory.⁽¹¹⁾ The light amplitude in the Fraunhofer diffraction pattern of any periodic array of N elements is:

$$U(X) = C \sum_{j=1}^N \int_{(j-1)p}^{jp} T_j(z) e^{-i2X[(j-1)(p - \frac{\Delta\phi}{2X}) + z]} dz \quad (1a)$$

where the deflection parameter X is

$$X = (\frac{\pi}{\lambda_g}) \operatorname{sinv} \quad (1b)$$

and C is a constant, j is an integer, λ_g is the mode wavelength in the deflector material, v is the diffraction angle, p is the period and $\Delta\phi$ is a voltage-induced phase difference between adjacent elements. The device is assumed to be operating in the near field so that the phase change over its length can be represented by $T_j(z)$, the transmission function of the j^{th} periodic element. (1a) can be written as:

$$U(X) = \sum_{j=1}^N e^{-i(j-1)(2pX - \Delta\phi)} F(T_j) \quad (1c)$$

where $F(T_j)$ is the Fourier transform of $T_j(z)$:

$$F(T_j) = \int_{(j-1)p}^{jp} T_j(z) e^{-i2Xz} dz \quad (1d)$$

The summation in (1c) represents the interference of identical diffraction patterns,

represented by $F(T_j)$, from successive elements. The intensity $I(X)$ is the square of the magnitude of $U(X)$. Upon evaluating the summation in (1c) we obtain an expression of the form

$$I(X) = (AF) (EF) \quad (2)$$

where

$$AF = \frac{\sin^2 N(pX - \frac{\Delta\phi}{2})}{\sin^2(pX - \frac{\Delta\phi}{2})} \quad (3)$$

and

$$EF = |F(T_j)|^2 \quad (4)$$

The array function AF is determined by the period of the array and the number of elements it contains and is independent of the phase distribution within any one element. The element function EF is the square of the magnitude of the Fourier transform of the transmission function at the output aperture of one element. The amplitude component of the transmission function is unity so for sufficiently simple phase distributions, the EF can be readily calculated.

(a) Consider first the single prism element of Fig. 1(a). The central sloping electrode produces, at least ideally, a linear phase slope across the wave, as in Fig. 1(b). The element is described by the transmission function T of its output aperture:

$$T = e^{i\phi_m [2z/p - 1]} \quad (5)$$

where $2\phi_m$ is the peak to peak phase shift across one element. The choice of such an ideal transmission function is shown to be useful for analyzing most aspects of device behavior. Later, a more complicated T is needed in order to discuss features such as crosstalk. If light propagates through the center of the device but with a beamwidth w which is less than p, the device width, then the Fourier integral across the beamwidth is:

$$F(T) = \frac{ipe^{-i\phi_m}}{2(pX-\phi_m)} e^{-i(pX-\phi_m)} \left(\frac{p+w}{p} \right) [1 - e^{i(pX-\phi_m)} \frac{2w}{p}] \quad (6)$$

For a single element, the AF in (3) is unity, so the intensity simply equals the EF. Hence, from (6), the intensity is:

$$I(X) = w^2 \frac{\sin^2 \left[\left(pX - \phi_m \right) \frac{w}{p} \right]}{\left[\left(pX - \phi_m \right) \frac{w}{p} \right]^2} \quad (7)$$

(b) Consider next an array of prism elements (Fig. 2(a)). The "prisms" may be all identical, resulting in a sawtooth phase distribution across the array, as shown in Fig. 2(b). Alternatively their phases may be staggered so that there is a phase shift $\Delta\phi$ between adjacent elements which results in a cumulative phase slope, as shown in Fig. 2(c). In either case, the j^{th} element is described by the transmission function:

$$T_j = e^{i[\phi_m((2z/p)-1) + (j-1)\Delta\phi - (j-1)2\phi_m]} \quad (8a)$$

where $\Delta\phi$ is zero if the prism phases are identical. The Fourier transform of

T_j is:

$$F(T_j) = \frac{ipe^{-i\phi_m}}{2(pX-\phi_m)} e^{-i2jpX} e^{i(j-1)\Delta\phi} [1 - e^{i2(pX-\phi_m)}] \quad (8b)$$

The EF (4) is then:

$$EF = p^2 \frac{\sin^2(pX - \phi_m)}{(pX - \phi_m)^2} \quad (9)$$

The intensity is obtained by substituting (9) and (3) in (2):

$$I(X) = \frac{\sin^2 N(pX - \frac{\Delta\phi}{2})}{\sin^2(pX - \frac{\Delta\phi}{2})} \cdot p^2 \frac{\sin^2(pX - \phi_m)}{(pX - \phi_m)^2} \quad (10)$$

(c) Finally, consider an array of channel waveguides (Fig. 3(a)). The phase of the wave emerging from any channel is regarded as constant, but differs from that of any other channel because of the linear variation in the lengths of the pairs of electrodes. An approximately linear phase slope is formed across the complete output wave, as indicated in Fig. 3(b). For the j^{th} channel the transmission

function is:

$$T_j = e^{i[(j-1)\Delta\phi]} \quad (11a)$$

where $(j-1)\Delta\phi$ is the electrooptically induced phase shift undergone by a wave propagating along the j^{th} channel and $\Delta\phi$ is here the phase difference between waves emerging from adjacent channels. The Fourier transform is formed:

$$F(T_j) = \frac{i}{2X} e^{i[(j-1)\Delta\phi]} e^{-i2X(j-1)p} (e^{-i2Xc} - 1) \quad (11b)$$

where c is the channel width. The EF simplifies to:

$$\text{EF} = c^2 \frac{\sin^2(cx)}{(cx)^2} \quad (12)$$

Substituting (12) and (3) in (2) gives the intensity:

$$I(X) = \frac{\sin^2 N(pX - \frac{\Delta\phi}{2})}{\sin^2(pX - \frac{\Delta\phi}{2})} \quad c^2 \frac{\sin^2(cx)}{(cx)^2} \quad (13)$$

From (7), (9) and (12) it is apparent that the EF has the same form for each deflector. For the single prism, if the beam entirely fills the prism width ($w = p$), then the EF is the same as that for a prism array (9). In the channel case (12), $\phi_m = 0$ and the beam aperture is c .

III. Deflection Characteristics: Number of Resolvable Spots

The nature of the deflection depends on whether the EF or the AF, or each, is displaced as a function of voltage. If a phase slope is created across the wave propagating through one element, then the resulting element pattern is deflected as a function of the voltage inducing the phase slope. If there is a phase difference between consecutive elements in an array, then the array pattern is deflected as a function of that phase difference. The nature of the deflection is summarized in Table I.

Consider the AF (3). It is a periodic series of narrow lobes. The zero order lobe is always maximum where $X = X_a$

$$X_a = \frac{\Delta\phi}{2p} \quad (14a)$$

This defines the phase, and hence voltage, controlled deflection of the zero order lobe from its original position when $\Delta\phi = 0$. Using (1b) to write (14a) in terms of the corresponding deflection angle v_a :

$$v_a = \sin^{-1} \left(\frac{\Delta\phi}{2\pi} \frac{\lambda g}{p} \right) \quad (14b)$$

The position of the central lobe of the EF (9) is phase dependent. The element pattern moves as the voltage is varied so that the maximum of the central lobe lies at $X = X_e$ where

$$X_e = \phi_m / p \quad (15a)$$

corresponding, from (1b), to a deflection angle v_e

$$v_e = \sin^{-1} \left(\frac{\phi_m}{\pi} \frac{\lambda g}{p} \right) \quad (15b)$$

Generally, the total number of spots, m , produced by any of the deflectors discussed equals twice (to allow for either polarity of voltage) the voltage-dependent deflection (X_a or X_e) divided by the spacing between adjacent spot positions. If the original spot is also included, the total number of spots becomes $(m + 1)$.

(a) Single prism element

The output intensity distribution (7) is deflected continuously as a function of voltage, as indicated in Fig. 4. Following the Rayleigh resolution criterion, that two spots are just resolved when the maximum of the spot at one angular position corresponds to the first zero (minimum) of a spot at the adjacent position, then the number of resolvable spots m is determined by X_e divided by the spacing π/w between the main maximum and first zero of the element diffraction pattern, namely:

$$m = \frac{2\phi_m}{\pi} \frac{w}{p} \quad (16)$$

A linear sloping electrode does not produce an exactly linear phase slope. However, over the center part of the element aperture, the induced phase shift is almost linear and can be determined by integrating the applied electric field along the length of the element.⁽²⁾ Extending the central fit to either end of the element gives:

$$\phi_m = \frac{4n^3 r_{ij} v}{\lambda \tan \psi} \quad (17)$$

where n is the refractive index, r_{ij} is the appropriate electro-optic coefficient for the crystal orientation used, λ is the free space wavelength (we use $\lambda = 0.6328 \mu m$) and ψ is the angle of the sloping electrode shown in Fig. 1(a). Using (17), the number of spots (16) can be written in terms of the applied voltage as

$$m = \frac{8n^3 r_{ij} w v}{\pi \lambda p \tan \psi} \quad (18a)$$

Alternatively, the voltage V_1 which produces deflection to the first spot position is:

$$V_1 = \frac{\pi \lambda p \tan \psi}{4n^3 r_{ij} w} \quad (18b)$$

It should be noted that the number of spots given by (18a) is larger by a factor of $4/\pi$ than that defined by Kaminow⁽²⁾ who divides the deflection angle by the angle between the $1/e^2$ points of a Gaussian beam.

(b) Prism array

The element pattern (9) of any prism array is deflected continuously as a function of voltage, through X_e , as shown in Fig. 5(a), (d). However, if the prisms are identical, the array pattern, in Fig. 5(b), does not move ($X_a = 0$ as $\Delta\phi = 0$), so the resultant intensity expressed by (10) is large only when the voltage is such that the main maximum of the element function is deflected to the angle corresponding to an array lobe, as in Fig. 5(c). The zeros of the EF then lie at the angles of all the other lobes, giving zero intensity except at the desired lobe (for an ideal device). Thus spots can be generated only at the discrete angles corresponding to the array lobes. The maximum number of spots is, therefore, twice the number of the maximum order to which light can be deflected. For any phase slope, m is determined by the integer part of $2X_e$ divided by π/p , the spacing between adjacent array lobes:

$$m = \frac{2\phi_m}{\pi} \quad (19)$$

which is identical to (16) for $w = p$. Introducing the voltage using (17) gives

$$m = \frac{8n^3 r_{ij} v}{\pi \lambda \tan \psi} \quad (20a)$$

The voltage V_1 is here

$$V_1 = \frac{\pi \lambda \tan \psi}{4n^3 r_{ij}} \quad (20b)$$

This requires that ϕ_m is π , i.e. the phase shift across any one element is 2π .

The corresponding deflection angle (in (15b) $\sin v_e \approx v_e$) is λ_g/p . For a single prism where $w = p$, (18b) reduces to (20b). As $\tan \psi$ approximately equals the period p divided by the length L , the voltage V_1 is proportional to p/L .

If the array consists of phase-staggered prisms, the intensity is described by (10) with $\Delta\phi \neq 0$. The position of the array pattern is now also voltage-dependent, as shown in Fig. 5(e). If the deflections of the element and array patterns are equal, i.e. $X_e = X_a$, then the output is continuously deflected.

The EF maximum always coincides with the zero order array lobe, as in Fig. 5(f), so all the spots are of equal intensity. The number of spots is increased by N relative to that for an identical prism array, corresponding to the $(N - 1)$ resolvable beam positions between consecutive array lobes where the intensity is now finite:

$$m = \frac{2N\phi_m}{\pi} \quad (21)$$

In terms of the voltage given in (17):

$$m = \frac{8Nn^3 r_{ij} V}{\pi \lambda \tan \psi} \quad (22a)$$

The voltage causing deflection to the first spot position ($X = \frac{\pi}{Np}$) is reduced by N to V'_1

$$V'_1 = \frac{\pi \lambda \tan \psi}{4Nn^3 r_{ij}} \quad (22b)$$

This requires that ϕ_m is π/N . The voltage V'_1 corresponds to a 2π phase shift across the entire array. The angle between adjacent spots is reduced by N , relative to that for the identical prism array, to λ_g/Np .

The condition of equal deflections, $X_e = X_a$, requires that $\Delta\phi = 2\phi_m$.

This is simply stating that there is a continuous linear phase shift across the entire device (see Fig. 2c), as would be the case for one large prism with the same phase shift. The intensity expression (10) simplifies to

$$I = p^2 \frac{\sin^2 N(pX - \phi_m)}{(pX - \phi_m)^2} \quad (23)$$

This is identical to the output intensity, denoted by (7), of a single prism, with a peak to peak phase difference $2N\phi_m$ across its width Np , which is completely filled by the beam. The staggered array and equivalent prism have identical deflection characteristics.

(c) Channel array

In this case the element function (12) is independent of voltage, so its position is fixed, as in Fig. 6(a). The AF (3), as shown in Fig. 6(b), is deflected continuously, because $\Delta\phi$ is finite. For unambiguous detection, the zero order lobe can move in one direction only as far as the undeflected position of the first order lobe, or, for $\pm V$, it can move in both directions through half this angle (see Fig. 6(c)). The deflection is continuous but the maximum useful deflection is through N resolvable positions, so the maximum number of spots is limited to the number of channels N . For spots of almost equal intensity the channel width should be small compared to the period so that the central lobe of the element pattern is very broad as in Fig. 6(a). If $c = p/4$, a spot at the undeflected position of the first lobe is 81% as intense as a spot at the zero lobe position; a spot midway between the lobes is 95% as intense.

For a given phase distribution, the number of spots m is determined by the deflection X_a divided by (π/Np) , the spacing between resolvable beam positions.

$$m = \frac{N\Delta\phi}{\pi} \quad (24)$$

This is identical to (21) for the staggered prism array, where $\Delta\phi = 2\phi_m$, or the single equivalent prism. Thus, for the same induced phase shift, these various deflectors produce the same number of resolvable spots.

The electric field in the channel, midway between the electrodes is given by⁽¹²⁾

$$E_z = \frac{2V}{\pi g} \quad (25)$$

where g is the gap between the electrodes. If L_j is the length of the electrode pair at the j^{th} channel, then the electrooptically induced phase shift undergone by a wave propagating along that channel is

$$\phi_j = \frac{2n^3 r_{ij} VL_j}{\lambda g} \quad (26)$$

As $\Delta\phi = (\phi_{j+1} - \phi_j)$, the number of spots in (24) can now be written in terms of the voltage in (26):

$$m = \frac{2n^3 r_{ij} VL}{\pi \lambda g} \quad (27a)$$

where L is the length of the longest electrode pair ($L = N[L_{j+1} - L_j]$).

Alternatively the voltage V_1 , causing deflection to the first spot position ($X = \frac{\pi}{Np}$), is given by

$$V_1 = \frac{\pi \lambda g}{n^3 r_{ij} L} \quad (27b)$$

The voltage V_1 corresponds to $\Delta\phi = 2\pi/N$, i.e. a 2π phase shift across the entire array. The angle between adjacent spots is $\lambda g/Np$, as for the staggered prism array. As in the prism case, V_1 is proportional to the element aperture (inter-electrode spacing g equals channel width c) divided by the length L . Thus the voltage per spot, and hence the drive power, are reduced in all the devices described by decreasing the prism or channel width, and by increasing the length.

TABLE I - Form of Deflection in Different Devices

NATURE OF ELEMENTS	ELEMENT FUNCTION	ARRAY FUNCTION	NATURE OF DEFLECTION
SINGLE PRISM	MOVES	UNITY	CONTINUOUS
ARRAY OF IDENTICAL PRISMS	MOVES	STATIC	DISCONTINUOUS
ARRAY OF PRISMS WITH STAGGERED PHASES	MOVES	MOVES	CONTINUOUS
ARRAY OF CHANNEL WAVEGUIDES	STATIC	MOVES	CONTINUOUS

IV. Design Considerations: Near Field Operation and Device Capacitance

The operation of any planar device is affected by the diffraction in the plane of the laser beam passing through it. We assume that the device size is optimized so that the near field region of the beam is contained within the device. This near field condition defines the minimum device aperture and hence the beamwidth, for the corresponding maximum device length. The minimum width of the Gaussian input beam, at one end of the device, is defined by:⁽¹³⁾

$$w_{\min} = \sqrt{\frac{4\lambda L}{\pi n}} \quad (28)$$

This is achieved when the beam is focused with its waist at the center of the device. For a device of length $L = 1$ cm and $n = 2.2$, $w_{\min} = 60.5 \mu\text{m}$. A single prism element of length 1 cm, and $\psi = 0.3^\circ$, has an aperture $(p-\ell) = 67.4 \mu\text{m}$, which just exceeds w_{\min} . A smaller angle ψ should not be used in a single element device of that length. In a channel waveguide array, where lateral confinement precludes diffraction, there are no such restrictions on device length.

Using conformal mapping methods, the device capacitance can be written as^(14,15)

$$C = \epsilon_0 (1 + \epsilon_r) \frac{K(\tau')}{2K(\tau)} \quad (29)$$

where C is the capacitance per unit length between two electrodes, ϵ_0 is the permittivity of free space (8.85 pF/m), ϵ_r is the relative permittivity, and $K(\tau)$ and $K(\tau')$ are complete elliptic integrals of the first kind, of modulus τ and τ' where $\tau' = (1 - \tau^2)^{1/2}$. Then for $K(\tau) < K(\tau')$, the elliptic functions can be written approximately,⁽¹⁴⁾ giving:

$$C = \frac{\epsilon_0 (1 + \epsilon_r)}{\pi} \ln \left[\frac{2\tau}{1 - (1 - \tau^2)^{1/2}} \right] \quad (30)$$

and for $K(\tau) > K(\tau')$:

$$C = \frac{\epsilon_0 (1+\epsilon_r) \pi}{4 \ln[2(\frac{1+\tau}{1-\tau})^{1/2}]} \quad (31)$$

For a periodic device,⁽¹⁵⁾ such as the prism elements, the parameter τ is given by:

$$\tau = \cos\left(\frac{\pi}{2(1+g/\ell)}\right) \quad (32a)$$

where ℓ is the width of the electrode line. For a two electrode device, such as a channel waveguide,

$$\tau = \frac{1}{1 + \frac{2\ell}{g}} \quad (32b)$$

The choice of the appropriate expression, (30) or (31), depends on the value of τ . For a periodic device, if $g \geq \ell$, $K(\tau) \geq K(\tau')$. In prism arrays, where the electrodes form a periodic structure, the gapwidth usually exceeds the linewidth and expression (31) is valid, with τ given by (32a). For a two electrode device, if $g \leq 5\ell$, $K(\tau) \leq K(\tau')$. In channel waveguide arrays, which are regarded as a series of two electrode devices, the gapwidth is small and expression (30) is valid with τ given by (32b).

The capacitance of channel waveguide devices is readily calculated as the interelectrode gap is constant. The total device capacitance C_t is given by

$$C_t = C \frac{NL}{2} \quad (33)$$

where L is the length of the longest electrode pair, at the last (N^{th}) channel. Only the capacitance across the channels between each pair of electrodes is considered; the gap between the adjacent electrodes of consecutive channels is considered to be large and the corresponding additional capacitance is neglected.

The electrode spacing in a prism device is continually varying. The capacitance C_1 of one prism element of length L must be written in terms of the variable g :

$$C_1(g) = 2C(g) L(g) \quad (34)$$

where $L(g)$ is the distance from one end of the device (where the gapwidth is a minimum g_1) to the point where the gapwidth is g . The gapwidth at the far end is given by g_2 . Then

$$L(g) = \left(\frac{g-g_1}{g_2-g_1}\right) L \quad (35)$$

For varying g , C_1 is obtained by deriving $\frac{dC_1}{dg}$ and then integrating it with respect to g along the length of the device:

$$C_1 = 2 \int_{\theta_1}^{\theta_2} [L(g) \left(\frac{dC}{d\tau} \frac{d\tau}{dg} \right) + \frac{CdL(g)}{dg} \frac{dg}{d\theta}] d\theta \quad (36)$$

where C is expressed by (31) (or 30) and $(d\tau/dg)$ is evaluated from (32a).

The parameter θ is given by $\cos^{-1}\tau$; hence

$$\theta = \frac{\pi}{2(1+g/\ell)} \quad (37)$$

and θ_1 and θ_2 correspond to g_1 and g_2 respectively. Then (31) gives as the capacitance C_1 :

$$C_1 = \frac{2\epsilon_0 (1+\epsilon_r) \pi L}{(g_2 - g_1)} \int_{\theta_1}^{\theta_2} \frac{1}{\ln[4(\frac{1+\tau}{1-\tau})]} \left[\frac{(g-g_1)}{(1-\tau^2)^{1/2} \ln[4(\frac{1+\tau}{1-\tau})]} - \frac{\pi\ell}{4\theta^2} \right] d\theta \quad (38)$$

Thus C_1 was computed from (38) by numerical integration. The total device capacitance C_t of an array of N identical prism elements is

$$C_t = NC_1 \quad (39)$$

For the phase-staggered prism array there is some additional capacitance corresponding to the electrode configuration devised to provide the phase differences by adding a phase delay $(j-1)\Delta\phi$ to the j^{th} element. In waveguide form, such a staggered array is a theoretical concept. It might be realized by forming channel waveguides in front of each prism element, the prisms themselves being identical, but with varying length electrodes placed along each channel in order to provide the appropriate phase delay. The lengths of the channel waveguide electrodes should be chosen so that the same voltage can be applied to each set of channel electrodes, to produce $(j-1)\Delta\phi$, and to each set of prism electrodes to produce a $2\phi_m$ phase difference across each element. Then ϕ_j , which is here the phase delay undergone by a wave propagating along the channel before the j^{th} prism element and is given by (26), must equal $(j-1)\Delta\phi$ or $(j-1)2\phi_m$, where ϕ_m is given by (17). No additional phase shift is required at the first element. Thus the length of the pair of electrodes at the j^{th} channel is given by L_j , where from (26) and (17);

$$L_j = (j-1) \frac{4g}{\tan\psi} \quad (40)$$

The corresponding capacitance CL_j is calculated from (30) and (32b), as for the channel waveguide arrays. If ΔC is the additional capacitance for the second element (corresponding to the channel electrode pair of length $4g/\tan\psi$), the total capacitance of a staggered prism device with N elements, constructed in this fashion, would be

$$C_t = NC_1 + \frac{N(N-1)}{2} \Delta C \quad (41)$$

It should be noted, that due to the addition of the channel electrodes, the total length of the phase-staggered prism array now exceeds L , the length of the identical prism array. For a prism device where $L = 1 \text{ cm}$, $\psi = 0.3^\circ$ and $g = 5 \mu\text{m}$,

the additional length corresponding to ΔC is 3.82 mm, so the total device length is $[1 + 0.382 (N-1)]$ cm, e.g. 2.53 cm for $N = 5$. The beamwidth considerations for near field operation do not change since no diffraction occurs in the channels. We neglect the length required to expand each phase shifted beam from its channel width c to the prism width p for $p \gg c$.

In Table II we compare experimental and theoretical capacitances of various devices in LiNbO_3 . We take $r_{ij} = r_{33} = 30 \times 10^{-12}$ m/V, $n = n_e = 2.2028$ and $\epsilon_r = \sqrt{\epsilon_1 \epsilon_3}$ or $\sqrt{\epsilon_2 \epsilon_3}$ which equals $\sqrt{78 \times 32}$ at the low frequencies of measurements. [At high frequencies, well above the acoustic resonances of the sample, ⁽¹⁶⁾ $\epsilon_r = \sqrt{43 \times 28}$, which is used in later bandwidth calculations.] In (a) we compare three different prism element designs fabricated in x-cut, y-propagating LiNbO_3 . For each $L = 9$ mm, $\ell = 5 \mu\text{m}$ and $g_1 = 5 \mu\text{m}$. However, different shapes were used for the central electrode: $\psi = 0.6^\circ$ in device (1), making the period $p = 114 \mu\text{m}$, and $\psi = 0.3^\circ$ in device (3), giving $p = 67 \mu\text{m}$. In device (2), indicated in Fig. 7, the electrode slope was increased from 0.4° along the central portion to 1.2° at either end, giving $p = 114 \mu\text{m}$ as in (1). The aim of this "dog-leg" electrode was to induce a linear phase slope across the full element width, and so reduce any crosstalk or sidelobes which would result if parts of the beam were deflected by different amounts. The phase slope created by a straight, angled electrode is steepest at either edge of the element width, where the small inter-electrode spacing makes the electric field strongest. ⁽²⁾ To compensate for this, the electrode was sloped in the opposite direction. Table II(a) shows the average capacitance of four samples measured at 1 KHz. The values are in close agreement with the computed values, and the capacitance of (2) is slightly less than that of (1). Table

II(b) shows the capacitance calculated for two channel arrays for which measured values are reported in the literature.^(7,8) The values agree well, with the measured values slightly exceeding the computed ones, probably due to the capacitance between adjacent electrodes of consecutive pairs.

For each deflector the capacitance increases linearly with length. However, the voltage per spot increases linearly with the inverse of length, so the requirements for high bandwidth (small L) and low drive power (large L) are conflicting.

TABLE II

(a) Capacitance of Array of 5 identical prism elements.

Array Capacitance (pF) C_t	Design of Prism Element Forming Array		
	(1)	(2)	(3)
Experimental	9.9	9.5	11.3
Computed	10.4	10.1	11.0

(b) Capacitance of Array of Channel Waveguide Elements

Device of:	No. of Channels N	Length L(cm)	Capacitance C_t (pF)	
			Computed	Measured
Sasaki ^(a)	20	1.8	127	148
Saunier ^(b)	5	0.36	3.2	4.3

(a) Ref. 7; (b) Ref. 8

V. Device Performance Characteristics: Bandwidth and Power Related to Number of Spots

The 3 dB bandwidth Δf_{3dB} of the deflector is that frequency at which the voltage across the device is decreased by $1/\sqrt{2}$ from its peak value at D.C. (the power is halved); hence the number of spots is decreased by $1/\sqrt{2}$.

In terms of capacitance, the bandwidth Δf_{3dB} is: (17)

$$\Delta f_{3dB} = (\pi R C_t)^{-1} \quad (42)$$

where R is the terminal shunt resistance, which equals the resistance of the power supply (50Ω), and C_t is determined from either (33) for channel waveguide elements or (39) for identical prism elements or (41) for phase-staggered prism elements. Figure (8) shows the bandwidth Δf_{3dB} in terms of the number of elements N for the three different arrays. In the computations we use linewidth $\ell = 5 \mu m$ and device length $L = 1 cm$. In prism elements, the sloping electrode angle ψ was chosen to be 0.3° and the smallest inter-electrode spacing was $g_1 = 5 \mu m$. In channel waveguide arrays, the gapwidth g was $5 \mu m$. In Fig. 8, the difference between the curves for identical and phase-staggered prisms is due to the channel elements added to produce the phase shifts in the latter.

A bandwidth criterion more appropriate to deflector performance is defined as that frequency up to which the device can be operated with no reduction in the number of resolvable spot positions. Any increase beyond Δf causes the number of spots at D.C. to be reduced by one. In practice, we consider both polarities of voltage, so Δf is the limiting frequency before the loss of two spots, i.e. m becomes $(m-2)$. In a continuous deflector the supply voltage

corresponding to the highest order spot causes a deflection at frequency Δf to halfway between the D.C. spot position and the D.C. position of the adjacent lower spot. For a discrete deflector, Δf corresponds to a reduction in voltage which results in the deflection of half the input beam intensity to the original spot position and half to the adjacent lower spot position. For each kind of deflector, this means that the voltage V_m is reduced to $\frac{1}{2} [V_m + V(\frac{m}{2} - 1)]$ where V_x is the voltage required for complete beam deflection to the x^{th} spot position. (For $\pm V$, there are $\frac{m}{2}$ spots to either side of the zero spot position.) Alternatively, for each deflector, the optical power received at a detector centered at the position of maximum deflection at D.C. is halved, so that it equals the power received at the detector at the next lower spot position.

The bandwidth Δf is:

$$\Delta f = F(m) \Delta f_{3\text{dB}} \quad (43a)$$

where

$$F(m) = \frac{(2m-1)^{1/2}}{(m-1)} \quad (43b)$$

Figure 9 shows $F(m)$ as a function of m . The 3 dB bandwidth $\Delta f_{3\text{dB}}$ depends only on the deflector geometry, so for any design it is a unique function of the number of elements N . However, the bandwidth Δf depends on the number of spots as well as the geometrical design. By using Fig. 9 to determine $F(m)$ for a chosen m and using Fig. 8 to determine $\Delta f_{3\text{dB}}$ for a chosen N , we can calculate Δf from (43) for any deflector.

The power P consumed by the device is:

$$P = V^2/R \quad (44)$$

where V is the D.C. or rms A.C. voltage. From (43) and (44) the drive power per unit bandwidth for the device, $P/\Delta f$, is:

$$P/\Delta f = \pi C_t V^2 / F(m) \quad (45)$$

We consider $P/\Delta f$ to be a more useful deflection criterion than the conventional $P/\Delta f_{3dB}$ obtained from (42) and (44) and which is smaller than $P/\Delta f$ by the factor $F(m)$.

The power required by different deflectors can also be compared qualitatively by considering the induced phase shift necessary for one spot position ($m=2$). From (16) and (19), for a single prism with $w = p$ and an array of identical prisms respectively, the peak to peak phase shift $2\phi_m$ across the device must equal 2π to produce a deflection through one spot position. From (21) and (24), for an array of phase-staggered prisms and an array of channel waveguides respectively, the phase difference $\Delta\phi$, between a point on one element and the corresponding point on the next element, must equal $2\pi/N$ for one spot, i.e. the necessary phase slope is now dependent on the number of elements, and is reduced by the factor N from that for the first set of devices. Quantitatively the powers used by the staggered prism array and the channel array are different. This is due to the different configuration used to induce the phase shift, and because spots produced by the channel device are limited to the number of channels, N . Also, in the channel case, as the length of the longest electrode, L , is kept constant, irrespective of N , the voltage per spot is independent of N as shown by (27b). In the staggered prism case, the voltage per spot is inversely proportional to N as shown by (22b).

Figure 10 shows the required drive power P as a function of the number of spots m , enabling comparison of different deflector structures. P is calculated from (44), where V and m are related by (18a), with $w = p$, for single prisms, (20a) for identical prism arrays, (22a) for phase-staggered prism arrays and (27a) for channel arrays. The bandwidth of the device described by each curve

can be determined from Figs. 8 and 9. In the prism devices, the angle of the sloping electrode ψ was 0.3° , unless otherwise indicated. If an array is composed of identical prism elements, then the addition of elements does not change the power characteristics of the single prism element. (For a single prism where the beam is narrower than the aperture, the power is greater by $(p/w)^2$.) The voltage per spot is independent of N as in (20b). The only gain is that the width of the spots is inversely proportional to N so the resolution of the spots is increased. However, if an array is constructed of phase-staggered prism elements then the power per spot decreases as elements are added, because P is proportional to $1/N^2$. The disadvantage of such an array is seen in Fig. 8, i.e. the bandwidth decreases very rapidly as N increases because of the capacitance associated with the channels proposed for staggering the phase slope. In any prism device, the power per spot increases quadratically as the electrode slope ψ is increased. By comparison, the reduction in capacitance with increasing ψ is very slight. In order to produce many spots with reasonable drive powers, ψ , and hence the prism width, must be small. Considering the single prism, or an identical prism array, the power per spot is independent of length if ψ is kept constant. Thus the same power curve (d) in Fig. 10 is obtained for prisms with $L \geq 1$ cm.

Different devices are compared in Fig. 11 where the power per unit bandwidth $P/\Delta f$, which is the most useful figure of merit for a deflector, is plotted versus the number of spots m . In prism devices a small ψ is wanted for low $P/\Delta f$. A single prism element is to be preferred to an array made up of such identical elements, because its bandwidth is higher and $P/\Delta f$ is lower.

However, an array composed of phase-staggered prism elements is better than a single element because $P/\Delta f$ decreases as the number of elements N increases. A staggered array is equivalent to a large prism with a phase shift across it equal to N times that across one element of the array; the voltage applied to the single prism would then be N times that applied to the whole array. In Fig. 11 the two devices are compared for the same number of spots, and $P/\Delta f$ is much higher for the large prism than for the corresponding array, the difference increasing with N . The $P/\Delta f$ characteristic of a channel waveguide array is plotted as a single curve for all $N = m$. Except for small m , the channel array is much less efficient than the arrays of phase-staggered prisms and is also worse than a single prism element, or an identical prism array where N is small.

Table III shows the power, bandwidth and $P/\Delta f$ for the various deflectors when producing 32 spots (which would allow 5 bits of resolution in analog to digital conversion). For devices where the power is unrealistically high, we show in parentheses the number of spots corresponding to a maximum applied power of 50W. In the prism devices the smallest interelectrode gap is 5 μm , so 50W corresponds to a maximum electric field of 10^5 V/cm , which is the approximate dielectric strength of LiNbO_3 . (In some channel devices $g = 10 \mu\text{m}$ and 200W is the corresponding power.) The channel device bandwidth might be improved by increasing the electrode spacing g ; however, the corresponding increase in power increases $P/\Delta f$ and the bandwidth Δf does not exceed ~60 MHz for $L = 1 \text{ cm}$. The bandwidth of a single prism element is over an order of magnitude higher (960 MHz for the same length). As N increases, the bandwidth decreases more rapidly for the staggered-phase prisms than for the

identical prisms. The power required by the staggered prism array and the channel array are of the same order of magnitude, whereas that used by the identical prism array or a single prism is approximately an order of magnitude greater. The relatively low $P/\Delta f$ for a single prism is determined by the high bandwidth. A large number of spots and an almost 1 GHz bandwidth can be achieved only with a single prism device, where the drive power is very high. The power is much lower in the phase-staggered prism array or the channel waveguide array; of these two, the former has the greater bandwidth at large numbers of spots. The restriction on the bandwidth of a channel device is a fundamental limitation which is due to the fact that the number of channel elements must be as large as the number of resolvable spots required. The bandwidth of every device might be proportionately increased if R were reduced by using a wideband impedance transformer with the 50Ω source.

TABLE III - Comparison of Figures of Merit of Various Deflectors.

(where $R = 50\Omega$, $L = 1 \text{ cm}$, and, in prism elements, $\psi = 0.3^\circ$ and $\ell = g_1 = 5 \mu\text{m}$.

Type of Device	Number of Elements N	Voltage per spot V_1 or V'_1 (V)	Power P (for 32 spots) (W)	(No. of spots for 50N)	$\frac{3}{dR}$	Bandwidth Δf (for 32 spots) (MHz)	$\frac{P}{\Delta f}$ (for 32 spots) (mK/MHz)
Single Prism	1 1 ($L = 2 \text{ cm}$)	8.12 8.12	337 337	(12) (12)	3745 2290	959 586	352 575
Identical Prism Array	2 3 4 5	8.12 8.12 8.12 8.12	337 337 337 337	(12) (12) (12) (12)	1872 1248 936 749	479 320 240 192	703 1055 1407 1758
Phase-staggered Prism Array	2 3 4 5	4.06 2.71 2.03 1.62	84.3 37.5 21.1 13.5	(24)	1467 804 512 356	376 206 131 91.0	224 182 161 148
Channel Waveguide Array N = 32	$\ell = g = 5 \mu\text{m}$ $\ell = 5, g = 10 \mu\text{m}$ $\ell = 2.5, g = 5 \mu\text{m}$ $\ell = 2.5, g = 10 \mu\text{m}$	3.10 6.20 3.10 6.20	49.2 197 49.2 197	(16) (16)	161 197 197 240	41.2 50.4 50.4 61.4	1193 3902 976 3207

VI. Experimental Comparisons

Table IV compares experimental and computed deflection parameters for the three designs of identical prism array for which capacitances were given in Table II(a). The voltage per spot V_1 is computed from (20b) or measured directly. The experimental angle between adjacent spots ψ_1 is derived from measurements of the deflected beam upon emerging from the LiNbO_3 sample. The data shows that the deflection behavior of the identical prism arrays is well described by the array theory and the approximate sawtooth phase waveform assumed for the aperture transmission function. The measured voltages per spot (V_1) are reasonably close to, and generally smaller than, the theoretical values. The dog-leg electrode design in device (2) does reduce the voltage per spot compared to device (1) which has the same period. (The angle ψ of the central part of the dog-leg was used in the computation for (2)). A closer fit between the measured and computed voltage per spot values is obtained if the basic sawtooth phase wave $\phi(z)$ is modified as in Fig. (12i). The phase slope is not created across the entire element width, because of the finite electrode linewidths. Here, it is assumed to be induced across the full width of the sloping electrode, i.e. $(p-\ell-2g_1)$, so it is steeper than when assumed to be across p . The voltage V_1 is reduced by $(p-\ell-2g_1)/p$, giving the values shown. The modified V_1 of device 2 is determined by theoretically extending the center part of the sloping electrode along the full length of the element. Alternatively, the linear fit⁽²⁾ used to give (17) for ϕ_m is exact over only the central 40% of the element width. Near the edges the actual phase slope is steeper. A closer fit to the phase

distribution over most of the width is obtained by taking a linear slope where the maximum phase is $1.25 - 1.5 \phi_m$. This choice reduces the V_1 values first computed by 20-33%.

Table V gives a comparison of the voltage per spot calculated from (18b) for (a), from (20b) for (b) and from (27b) for (c), (d), (e), and the measured voltages of various waveguide devices reported in the literature.^(2,4,7,8,9) There is generally good agreement. In (a) the value of 50V would give the $1/e^2$ resolution between spots mentioned in Section III(a). It is derived by Kaminow⁽²⁾ from 30V, which is demonstrated to give two spots; 50V is greater by $4/\pi$ than the calculated V_1 , as would be expected from III(a). The V_1 value in (c) is determined using (27b) where the voltage is effectively halved (or the length doubled) because there are two sets of electrodes. With the 20 channel device it is estimated that 16 spots can be resolved (5 are shown). The voltages for (d) and (e) are calculated assuming equal line and gapwidths. Expression (27b) for V_1 , corresponds to that used by Sasaki⁽⁷⁾ but is greater by $\pi/2$ than that stated by Tsai,⁽⁹⁾ because of the factor $2/\pi$ in the electric field expression (25).⁽¹²⁾

TABLE IV - Deflection parameters of arrays of identical prisms (N = 5).

	Device		
	(1)	(2)	(3)
<u>Design</u>			
ψ (deg.)	0.6	0.4	0.3
p (μm)	114	114	67
<u>Computed</u>			
v_1 (V)	16.2	10.8	8.1
$\frac{v_1(p-\ell-2g_1)}{p}$ (V)	14.1	9.4	6.3
$v_1 = \sin^{-1}(\frac{\lambda}{n_e p})$ (deg.)	0.14	0.14	0.25
<u>Experimental</u>			
v_1 (V)	15.8	8.4	6.3
v_1 (deg.)	0.14	0.14	0.24

TABLE V. Voltage per spot for various prism and channel deflectors.

Device	No. of elements N	Voltage per spot V_1 (volts)	
		Calculated	Measured
(a) Single Prism ^a	1	39	50
(b) Identical prism array ^b	4	22	16 (<u>+8</u>)
(c) Channel Wave-guide array ^c	20	1.7	2.1
(d) Channel Wave-guide array ^d	5	6.5	3.1
(e) Varying length, interdigital electrode array on planar waveguide ^e		8.4	6

a. Kaminow Ref. 2; b. Tsai Ref. 4; c. Sasaki Ref. 7;
 d. Saunier Ref. 8; e. Tsai Ref. 9.

VII. Crosstalk

The simple phase waveform of Fig. (2b) and its resulting EF are not adequate for predicting crosstalk as they would produce zero crosstalk. In a single prism element, the input beam can be focused so that it propagates only across the region where there is an approximately linear phase slope. All the beam should then be deflected by the same amount, so any distortion of the beam or crosstalk between different spot positions would be negligible. In a prism array, there are narrow regions of the beam across which a constant phase shift (no phase slope) would be generated, and the phase slope would not be linear across the remainder of the beam. Hence small parts of the beam would not be deflected, while other parts would be deflected through different angles, resulting in crosstalk between the various spot positions.

The waveform in Fig. (12i) is a better representation of the phase distribution induced across the beam by the electrooptic prism array and is more useful for predicting crosstalk. It assumes zero electro-optic phase shift of the parts of the wave propagating under the straight electrodes lying along the crystal axis, and constant phase shift across the parts of the wave propagating between the straight electrode and the edge of the sloping one, i.e. within the gaps g_1 . The EF corresponding to this waveform is more complicated than (9) and is given in the Appendix. The main term, S_2^2 , is of the same form as the desired expression (9) but other significant terms of different periods are added. Also, the lobes of the EF are broadened so that

the central lobe now has a halfwidth $\frac{\pi}{(b-t)}$, rather than π/p . Thus the EF zeros no longer coincide with the AF zeros, and the finite magnitude of the EF at the location of the AF lobes results in crosstalk. Hence, in an identical prism array, there would be crosstalk between the various spot positions and the spots would be broadened. For a single prism element the number of spots would be reduced, by approximately $(b-t)/p$, because of the EF broadening. In a phase-staggered prism array, the number of resolvable spots would be reduced because of this broadening of the EF and hence of the spots. Crosstalk would be large only between the spot positions which coincide with AF lobes other than the desired one. Figure 12 shows the form of the EF deflected so that its maximum coincides with the first lobe of the AF. Curve (a) corresponds to the phase distribution (i), while (b) corresponds to the ideal sawtooth (ii), drawn for the same period. The lowering and broadening of the EF peak is evident.

In the channel waveguide array there would be distortion and broadening of the spots if there is a non-uniform light distribution across the channels or within the width c of any one channel. The EF is stationary and has a very broad central lobe, so any changes in it are less critical than in the prism case and do not lead directly to crosstalk. Crosstalk between the desired spot and immediately adjacent positions would result from broadening of the AF lobe, which would reduce the number of resolvable beam positions.

In the prism case, the magnitude of the EF (A_2) was calculated at angles corresponding to AF lobes, including the angle of the chosen EF deflection.

The crosstalk intensity between different spot positions is the product of the EF values with the AF which is the same at each lobe. Magnitudes determined from (A2) for the phase distribution of Fig. (12i) are shown in Table VI(a). In (b) are given some average measured values for prism arrays (1) - (3), which were obtained by scanning a narrow slit in front of a photomultiplier tube across the output deflection pattern. The crosstalk is generally smallest from spots of order higher than the desired order. The crosstalk becomes worse as the deflection angle increases, i.e. as the desired spot corresponds to a higher order lobe. Also the crosstalk becomes worse as the period of the device is decreased. To minimize crosstalk, a large angle ψ is desired. Unfortunately this requirement is opposite to that for reducing the voltage per spot and drive power. The computed crosstalk is smaller than that obtained experimentally. The magnitudes are computed from a phase waveform, Fig. (12i), which is still approximate as it does not allow for non-linearity in the phase slope. Also, the crosstalk is calculated from the EF sidelobes for an idealized waveguide device, with no in-plane scattering and no defects in the electrode photolithography. The deflectors tested were not perfect. Experimentally it could be seen that the crosstalk in device (2) was smaller than that in (1). The dog-leg electrode shape in (2) should make the phase shift linear over a greater portion of the element width, so that a greater part of the beam is deflected through the same angle. Figure 13 shows an output scan for device (2), where the beam is deflected to the third spot position. Further sophistication in electrode design would presumably result in improved crosstalk levels.

TABLE VI - Crosstalk (-dB) for identical prism array devices.

(a) Computed values

Between numbered and deflected spot positions	Deflection to 1st spot		Deflection to 5th spot	
	Device (1)	Device (3)	Device (1)	Device (3)
1			15.9	9.8
2	20.6	15.8	16.1	8.6
3	21.0	16.9	16.6	8.2
4	21.4	18.1	17.3	8.7
5	21.8	19.2		
6	22.3	20.2	19.4	12.6
7	22.8	21.0	20.9	16.5
8	23.3	21.8	22.7	22.8
9	23.8	22.6	24.8	37.9
10	24.3	23.8	27.2	32.4

(b) Measured crosstalk (-dB) between adjacent spots for deflection to first spot position.

Between spots	Device		
	(1)	(2)	(3)
0 and 1	6.6	8.3	5.1
2 and 1	8.0	10.0	6.2

VIII. Conclusions

Fraunhofer diffraction theory was used to analyze the far field output intensity distribution of three types of electro-optic waveguide deflectors: single prisms, arrays of identical and phase-staggered prism elements, and arrays of channel elements. The analysis reduces to determining the Fourier transform of the phase shift induced across the optical beam by the device, and allows each deflector to be characterized in a consistent manner. We found that first order approximations to the phase shifts result in reasonably complete descriptions of the voltage dependent deflection characteristics of the device. This approach shows clearly the nature of the deflection; in particular the discontinuous deflection produced by an array of identical prisms is evident. To calculate bandwidths for each type of device, we determined electrode capacitance values for the various interdigital structures, which have constant and varying interelectrode spacings. Agreement is very good with our measured values for prism arrays and with values in the literature for channel arrays. We introduce a bandwidth criterion, specific to deflector performance, within which there is no degradation in the number of resolvable spots. The deflectors are compared in terms of power, bandwidth and power per unit bandwidth, as functions of the number of resolvable spots. These three figures of merit are shown in Figs. 8-11 and Table III. We find that none of the devices analyzed appears promising for 5 bit analog-to-digital conversion applications (32 spots at high bandwidth and moderate power). Channel waveguide arrays have severe bandwidth limitations (< 100 MHz) while prisms and identical prism arrays have very high power requirements.

(~ 300W). Phase-staggered prism arrays use the lowest power per unit bandwidth, having the lowest powers (for \geq 3 elements) but only moderate bandwidths (~ 200 MHz for 3 elements). As an arrangement for staggering the phases is difficult to implement in waveguide form, we have analyzed these arrays only approximately.

Deflection parameters for our identical prism arrays and various devices in the literature agree reasonably well with computed parameters. Crosstalk ratios were computed for idealized, identical prism arrays, by modifying the simple sawtooth phase distribution. The measured crosstalk values are considerably larger. Also, in prism array deflectors, it was demonstrated experimentally that a modification in the linear sloping electrode design resulted in lower drive power, lower crosstalk and slightly increased bandwidth.

Acknowledgements

The author is grateful to W. K. Burns and T. G. Giallorenzi for useful discussions during the course of this research. We acknowledge the participation of A. F. Milton in the early stages of this project, and discussions with J. F. Revelli concerning the discontinuous nature of the identical prism deflection. Acknowledgement is also due to J. F. Bass, K. H. Boyle, G. V. Hodge and E. J. West for assistance in fabricating the prism deflectors.

Appendix

The transmission function of the j^{th} element defined by the phase distribution in Fig. (12i) has four parts:

$$T_j = T_{j1} + T_{j2} + T_{j3} + T_{j4} \quad (\text{A1})$$

where

$$T_{j1} = e^{-i[\phi_m - (j-1)\Delta\phi]} \quad ((j-1)p < z < [(j-1)p+t])$$

$$T_{j2} = e^{i[\phi_m(\frac{2z}{b-t}) - 1] + (j-1)\Delta\phi - (\frac{(j-1)p+t}{b-t})2\phi_m} \quad [(j-1)p+t] < z < [(j-1)p+b]$$

$$T_{j3} = e^{i[\phi_m + (j-1)\Delta\phi]} \quad [(j-1)p+b] < z < [(j-1)p+s]$$

$$T_{j4} = e^{i(j-1)\Delta\phi} \quad [(j-1)p+s] < z < jp$$

This describes an identical or a phase-staggered prism array. T_{j2} should be compared with T_j in (8a). For the most general case, $|F(T_j)|^2$ has four "magnitude squared terms" (of form $F_1 F_1^*$) and six pairs of crossterms (of form $F_1 F_2^* + F_1^* F_2$). In practice, the two regions of constant, finite ϕ would be of equal width, i.e. $t = (s-b)$. For this case the element function is:

$$\begin{aligned} EF = & 4\cos^2(bX-\phi_m)[S_1^2] + [S_2^2] + [S_3^2] + 4\cos(bX-\phi_m)[S_1][S_2] \\ & + 2\cos(pX)[S_2][S_3] + 4\cos(pX)\cos(bX-\phi_m)[S_1][S_3] \end{aligned} \quad (\text{A2})$$

where

$$S_1 = t \frac{\sin(tx)}{(tx)}$$

$$S_2 = (b-t) \frac{\sin[(b-t)x-\phi_m]}{[(b-t)x-\phi_m]}$$

$$S_3 = (p-s) \frac{\sin[(p-s)x]}{[(p-s)x]}$$

The intensity is given by the product of EF in (A2) and AF in (3). The array function is unchanged for a constant period p .

References

1. P. K. Tien, S. Riva-Sanseverino, A. A. Ballman, "Light beam scanning and deflection in epitaxial LiNbO₃ electro-optic waveguides," *Appl. Phys. Lett.*, 25, pp. 563-565, Nov. 1974.
2. I. P. Kaminow, L. W. Stulz, "A planar electrooptic prism switch," *IEEE J. Quantum Electron.*, QE-11, pp. 633-635, Aug. 1975.
3. V. J. Fowler, J. Schlafer, "A survey of laser beam deflection techniques," *Proc. IEEE*, 54, pp. 1437-1444, Oct. 1966.
4. C. S. Tsai, P. Saunier, "Ultrafast guided-light beam deflection/switching and modulation using simulated electro-optic prism structures in LiNbO₃ waveguides," *Appl. Phys. Lett.*, 27, pp. 248-250, Aug. 1975.
5. Y. Ninomiya, "Ultrahigh resolving electrooptic prism array light deflectors," *IEEE J. Quantum Electron.*, QE-9, pp. 791-795, Aug. 1973.
6. T. C. Lee, J. D. Zook, "Light beam deflection with electrooptic prisms," *IEEE J. Quantum Electron.*, QE-4, pp. 442-454, Jul. 1968.
7. H. Sasaki, R. M. De LaRue, "Electro-optic multichannel waveguide deflector," *Electron. Lett.*, 13, pp. 295-296, May 1977.
8. P. Saunier, C. S. Tsai, I. W. Yao, Le T. Nguyen, "Electrooptic phased-array light beam deflector with application to analog-to-digital conversion," in Technical Digest of Topical Meeting on Integrated and Guided Wave Optics, Salt Lake City, Utah, paper TuC2, Jan. 1978.
9. C. S. Tsai, P. Saunier, "New guided-wave acousto-optic and electro-optic devices using LiNbO₃," *Ferroelectrics*, 10, pp. 257-261, 1976.
10. R. A. Meyer, "Optical beam steering using a multichannel lithium tantalate crystal," *Appl. Optics*, 11, pp. 613-616, Mar. 1972.
11. M. Born and E. Wolf, "Principles of Optics," Pergamon Press, pp. 398-405, 4th edition, 1970.
12. D. Marcuse, "Electrooptic coupling between TE and TM modes in anisotropic slabs," *IEEE J. Quantum Electron.*, QE-11, pp. 759-767, Sep. 1975.
13. I. P. Kaminow, E. H. Turner, "Electrooptic light modulators," *Proc. IEEE*, 54, pp. 1374-1390, Oct. 1966.
14. N. Uchida, "Design and comparison of single-mode planar and ridge type electro-optic waveguide modulators," *Optical and Quantum Electron.*, 9, pp. 1-13, 1977.

15. J. S. Wei, "Distributed capacitance of planar electrodes in optic and acoustic surface wave devices," IEEE J. Quantum Electron., QE-13, pp. 152-158, Apr. 1977.
16. I. P. Kaminow, E. H. Turner, "Handbook of Lasers," (R. J. Pressley, ed.), p. 452, Chemical Rubber Company, Cleveland, Ohio, 1971.
17. F. S. Chen, "Modulators for optical communications," Proc. IEEE, 58, pp. 1440-1457, Oct. 1970.

Figure Captions

Figure 1 - Single Prism Element

- (a) Geometrical configuration (x- or y-cut LiNbO₃, to utilize r_{33})
- (b) Near field phase distribution electro-optically induced across wave after propagating through single prism element

Figure 2 - Array of prism elements (shown for N = 5; p much exaggerated compared to L)

- (a) Geometrical configuration
- (b) Near field phase distribution for array of identical prism elements
- (c) Near field phase distribution for array of phase-staggered prism elements

Figure 3 - Array of channel waveguide elements

- (a) Geometrical configuration
- (b) Near field phase distribution electro-optically induced across wave after propagating through array of channel waveguides

Figure 4 - Deflection behavior of single prism element: element function (7), equal to intensity, sketched as function of $X = \frac{n_e \pi}{\lambda} \sin v$

Figure 5 - Deflection behavior of prism array

- (i) prisms identical ($\Delta\phi = 0$)
 - (a) Element function (9) deflected through $X = \pi/p$
 - (b) Array function (3)
 - (c) Resultant intensity (10) where $\Delta\phi = 0$

(ii) prisms phase-staggered (non-identical, $\Delta\phi$ finite)

(d) Element function (9) deflected through $X = \frac{2\pi}{N_p}$

(e) Array function (3) deflected through $X = \frac{2\pi}{N_p}$, where

$$\Delta\phi = 2\phi_m$$

(f) Resultant intensity (10)

Figure 6 - Deflection behavior of channel waveguide array

(a) Element function (12)

(b) Array function (3) deflected through $X = 2\pi/N_p$

(c) Resultant intensity (13)

Figure 7 - Element of experimental, identical prism array device (2):

"dog-leg" electrode design

Figure 8 - Device 3 dB bandwidth plotted in terms of number of elements.

Element length $L = 1$ cm.

(a) ——— Array of identical prism elements ($\psi = 0.3^\circ$, $\ell = g_1 = 5 \mu\text{m}$)

(b) ———— Array of phase-staggered prism elements ($\psi = 0.3^\circ$, $\ell = g_1 = 5 \mu\text{m}$)

(c) ----- Array of channel waveguide elements ($\ell = g = 5 \mu\text{m}$)

Figure 9 - Bandwidth variable $F(m) = \Delta f / \Delta f_{3\text{dB}}$ plotted as function of number of resolvable spots.

Figure 10 - Drive power plotted as function of number of resolvable spots produced. Element parameters are as specified below, and below Fig. 8, unless otherwise indicated on graph.

(d) - - - Single prism element ($L = 1$ cm, $\psi = 0.3^\circ$, $\ell = g_1 = 5 \mu\text{m}$) or single large prism element ($L > 1$ cm, $\psi = 0.3^\circ$, $\ell = g_1 = 5 \mu\text{m}$).

The curves for (a) and (d), with the same ψ , here coincide.

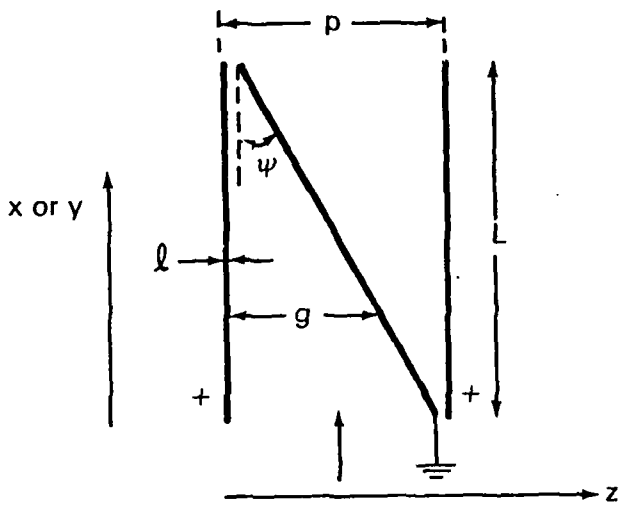
Figure 11 - Power per unit bandwidth plotted in terms of number of resolvable spots. Device parameters as for Figs. 8 and 10 unless otherwise indicated on graph.

Figure 12 - Element function deflected to first spot position (first lobe of array function)

- (a) is computed from (A2) for the transverse phase distribution (i),
for $p = 114 \mu\text{m}$, $s = 109 \mu\text{m}$, $t = 5 \mu\text{m}$;
- (b) is computed from (9) for the ideal phase distribution (ii)
[as in Fig. (2b)], for $p = 114 \mu\text{m}$.

Figure 13 - Scan of far field output intensity for identical prism array device (2); 26V applied; deflection to third spot position (third lobe of array function).

(a)



(b)

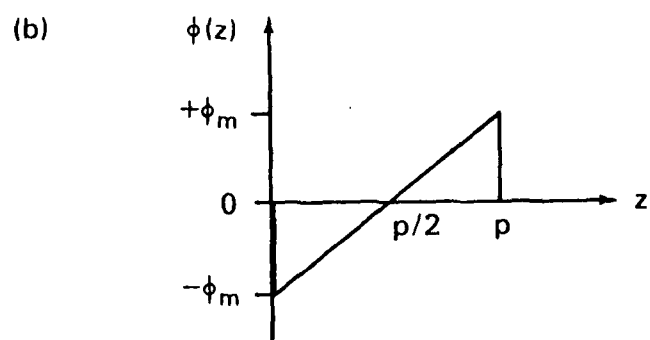


Fig. 1

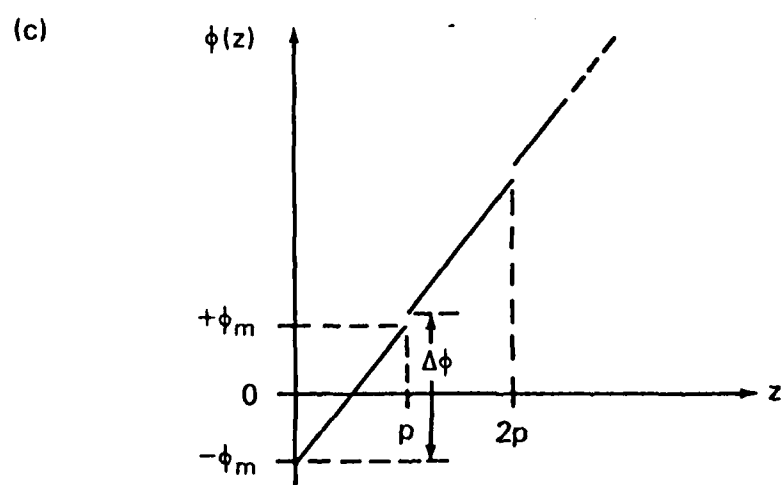
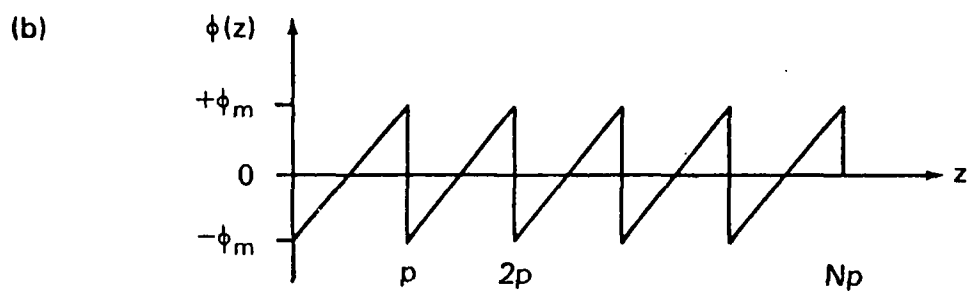
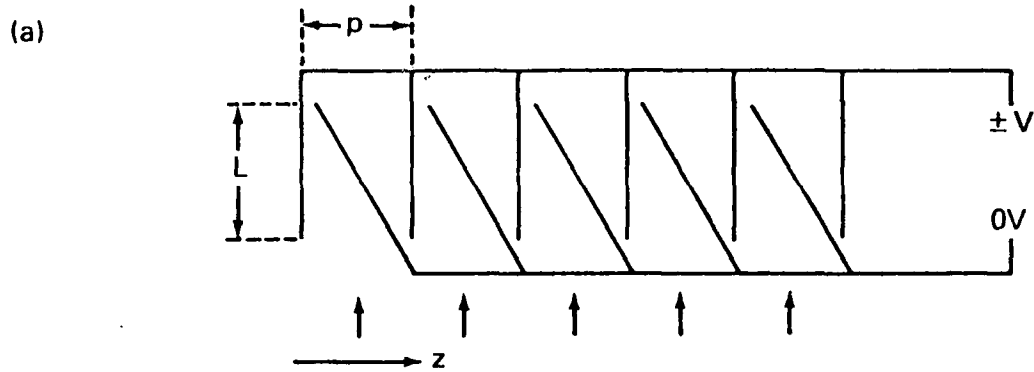
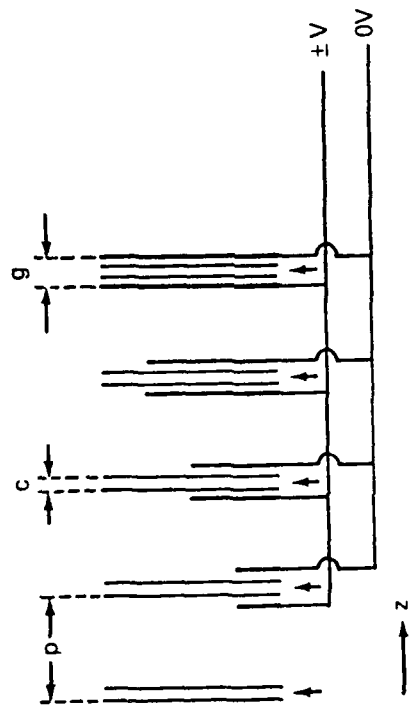


Fig. 2

(a)



(b)

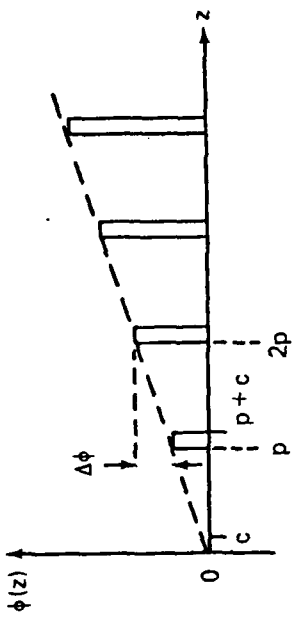


Fig. 3

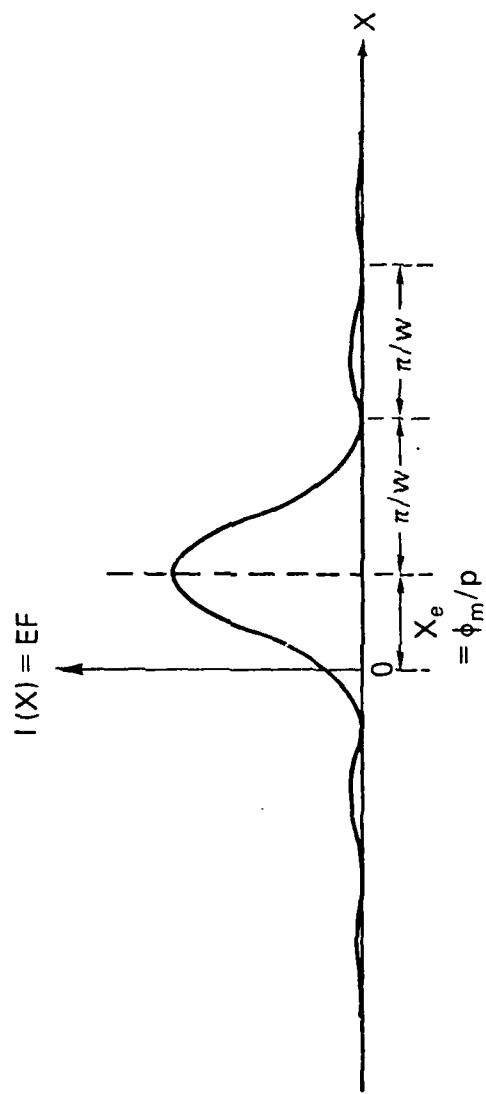


Fig. 4

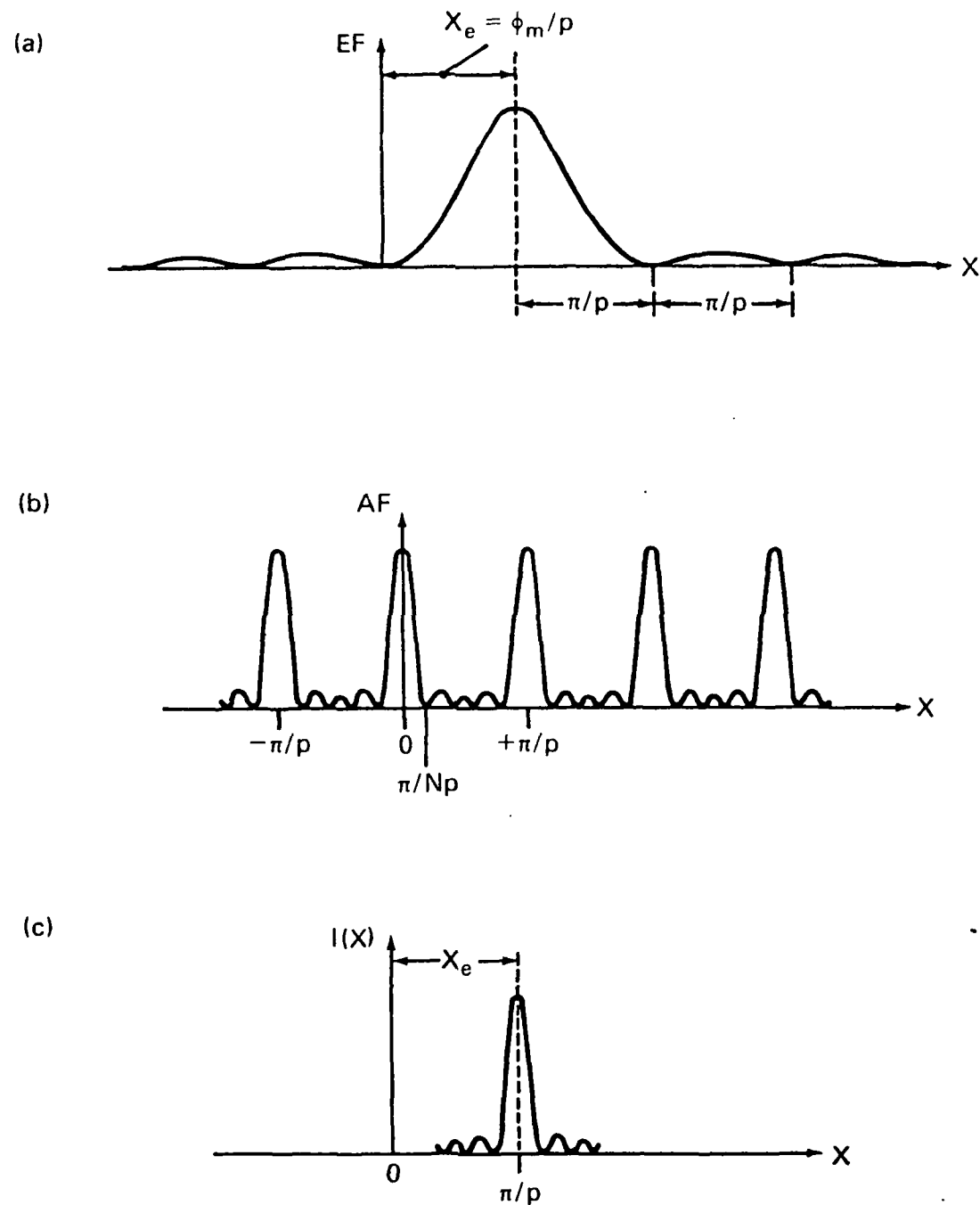


Fig. 5(i)

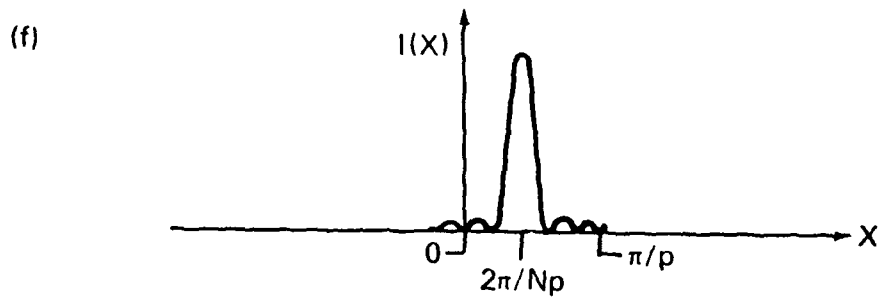
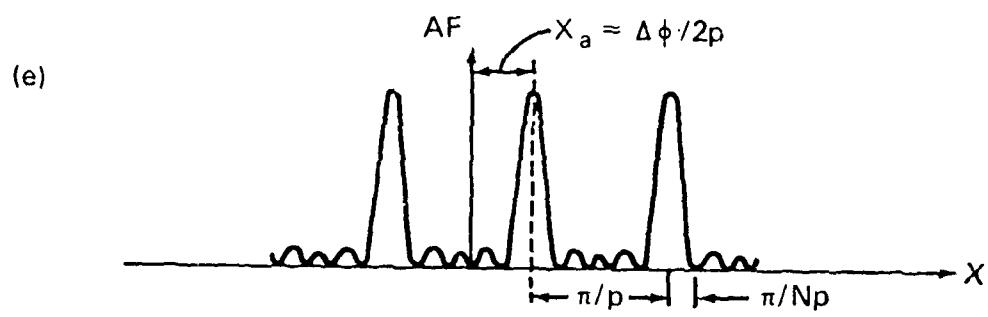
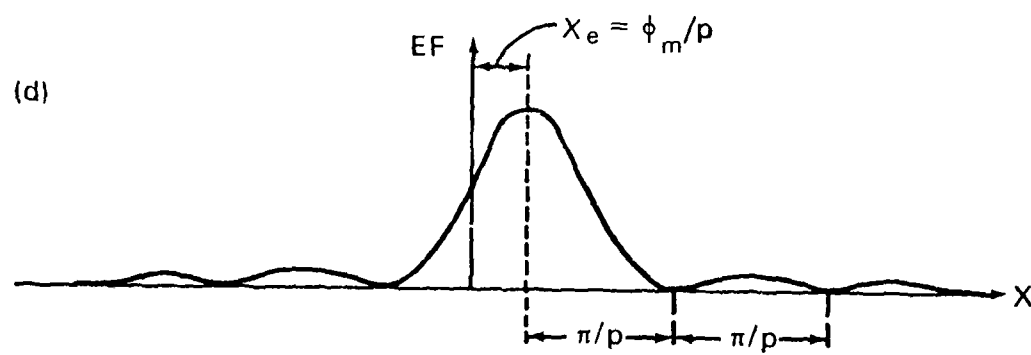


Fig. 5(ii)

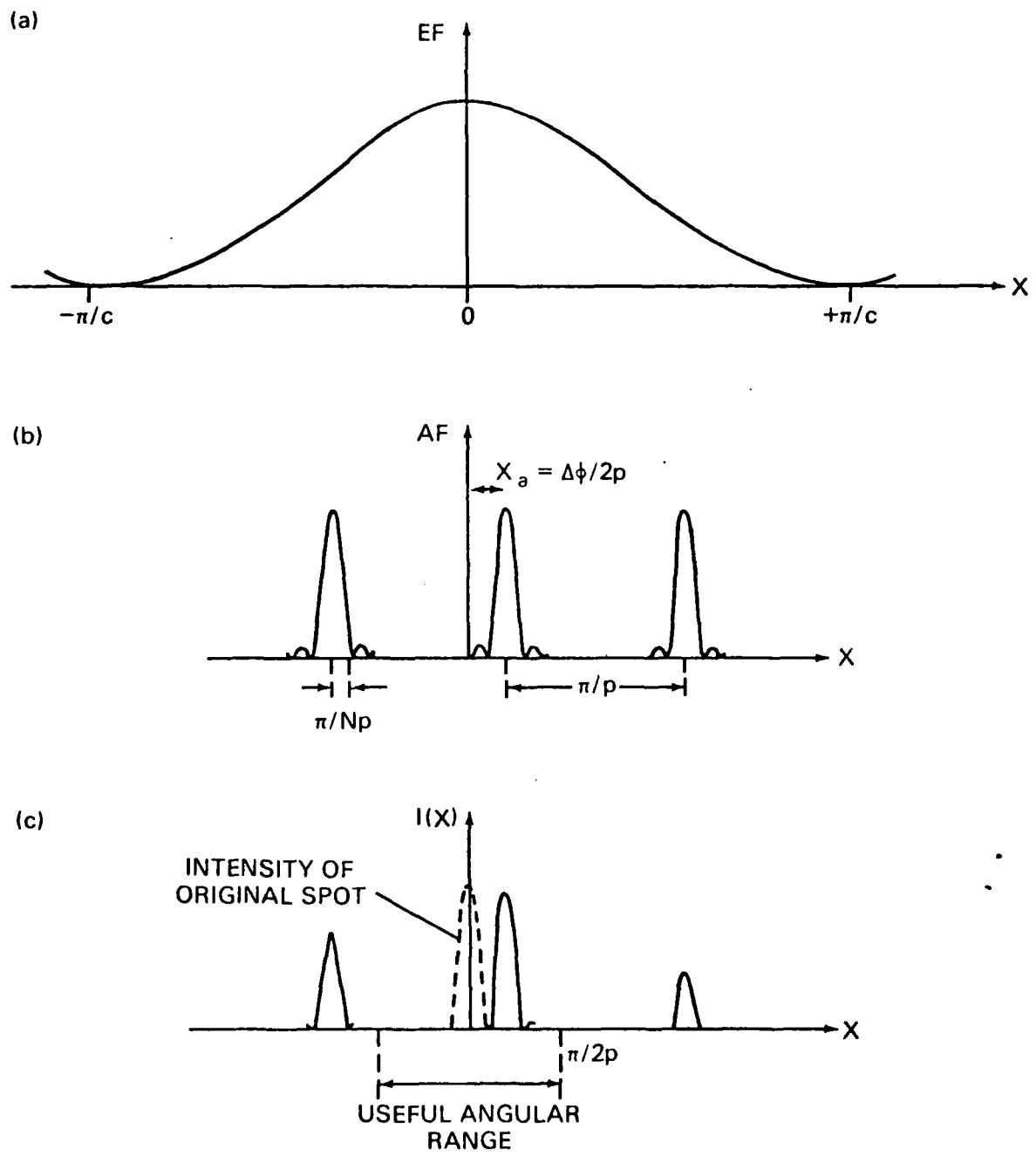


Fig. 6

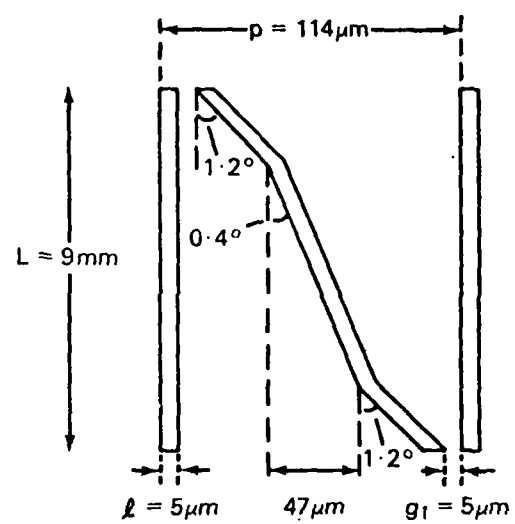


Fig. 7

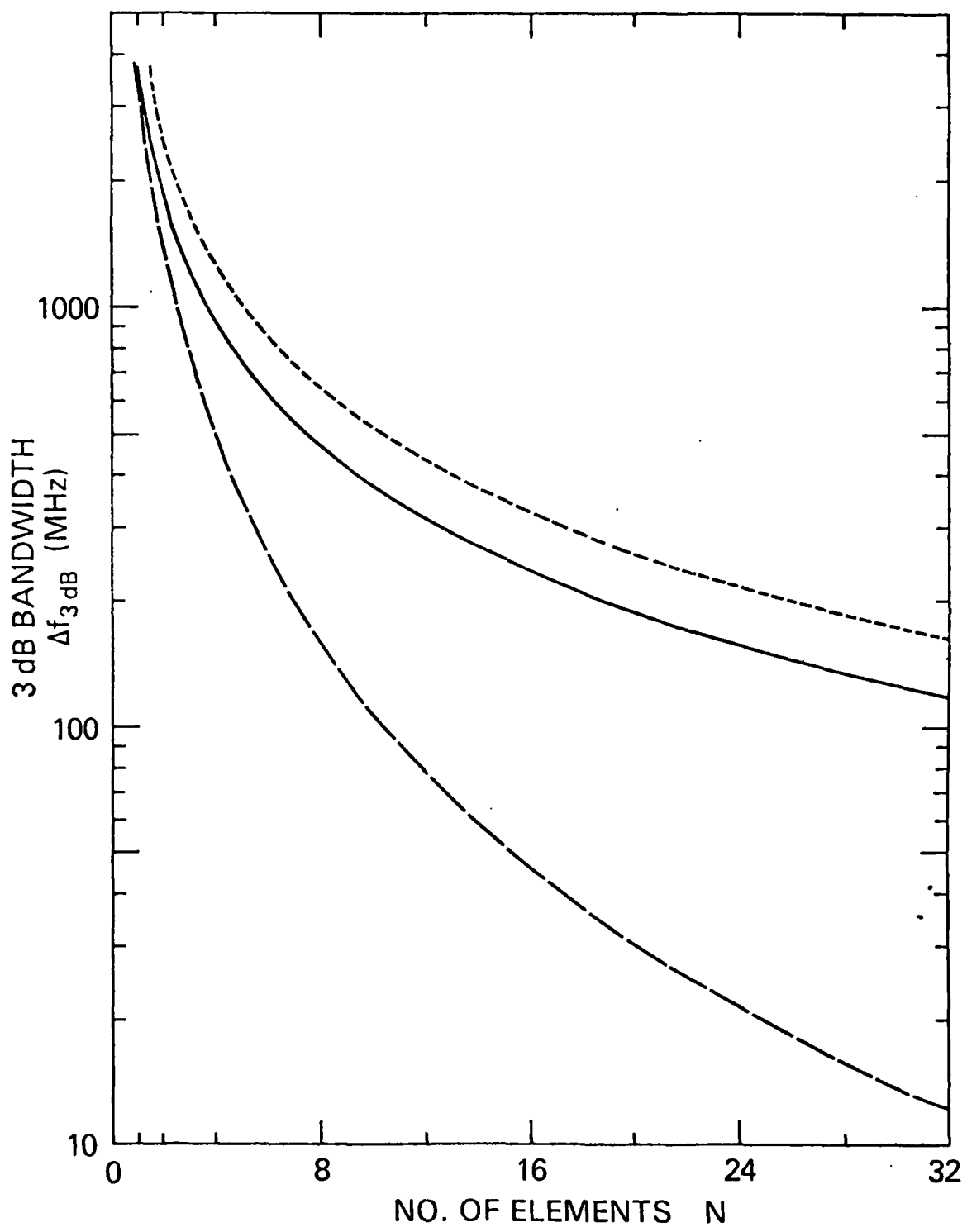


Fig. 8

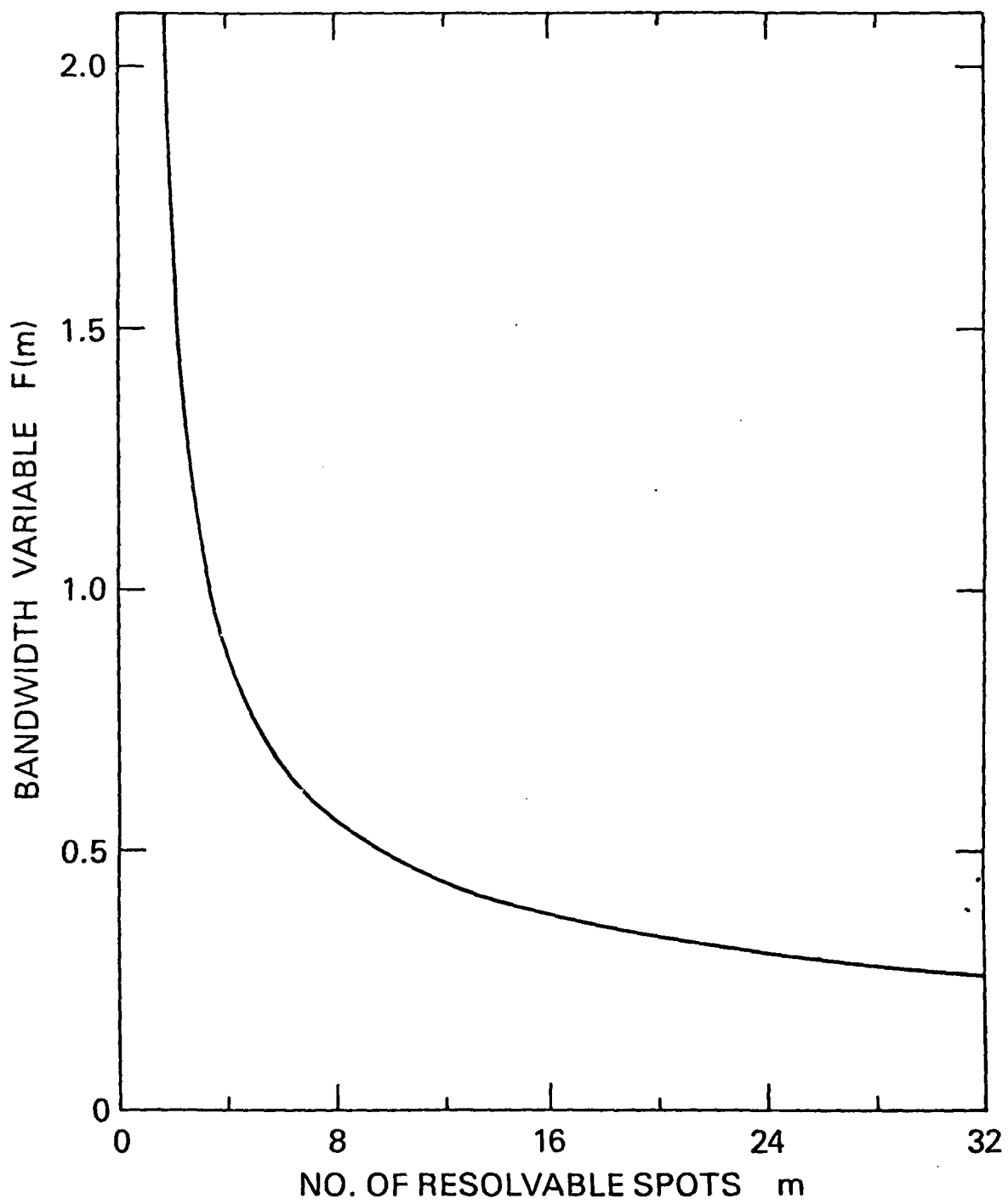


Fig. 9

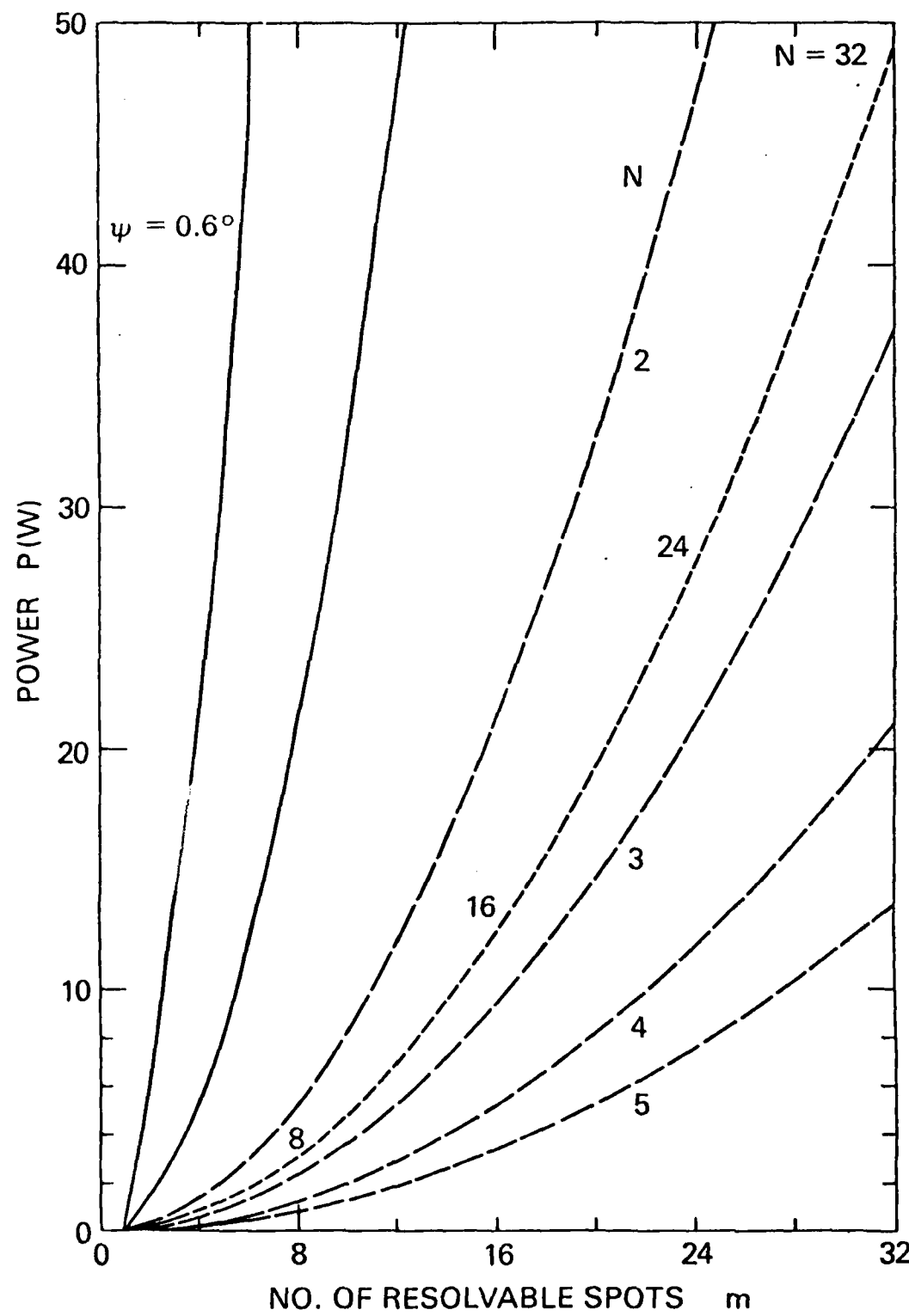


Fig. 10

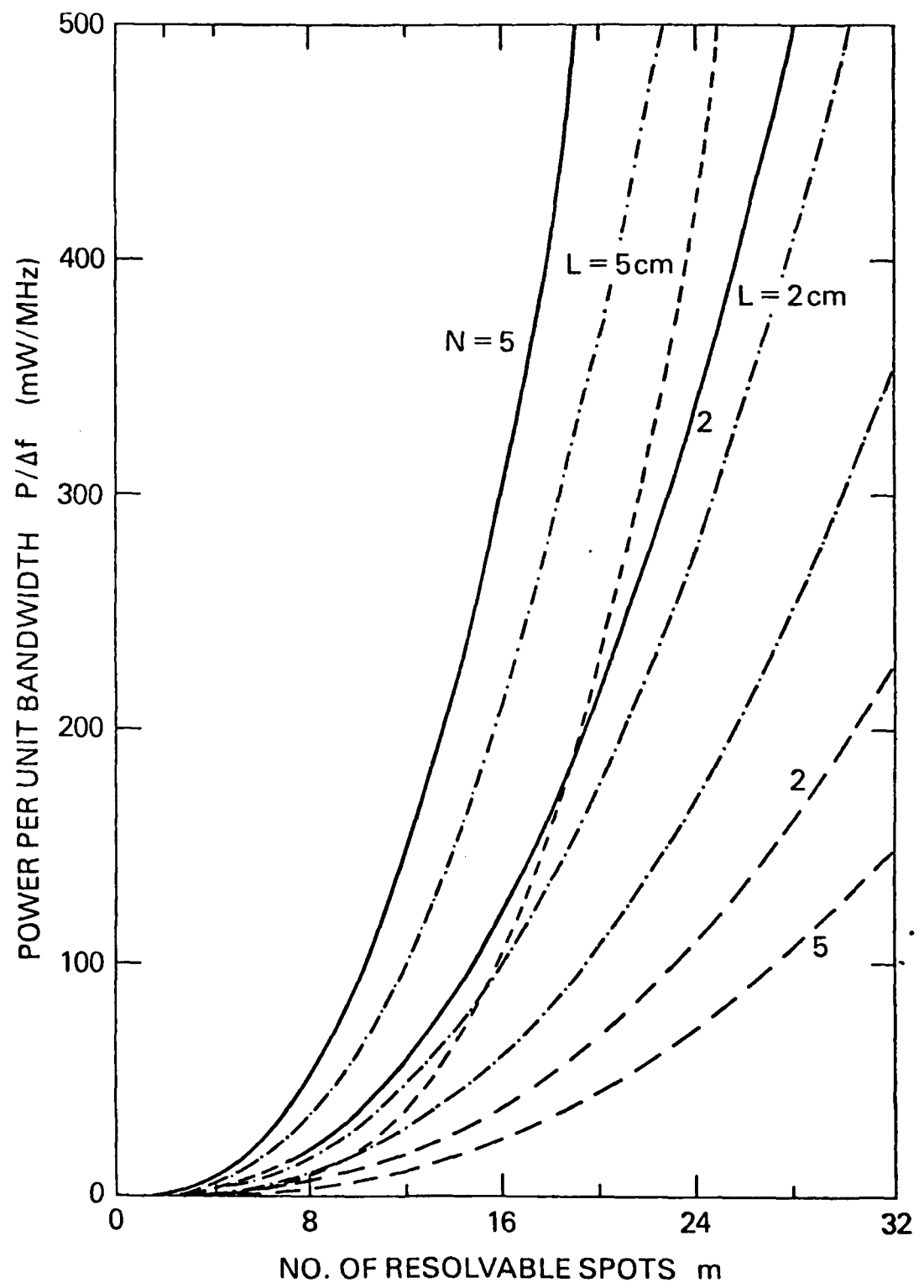


Fig. 11

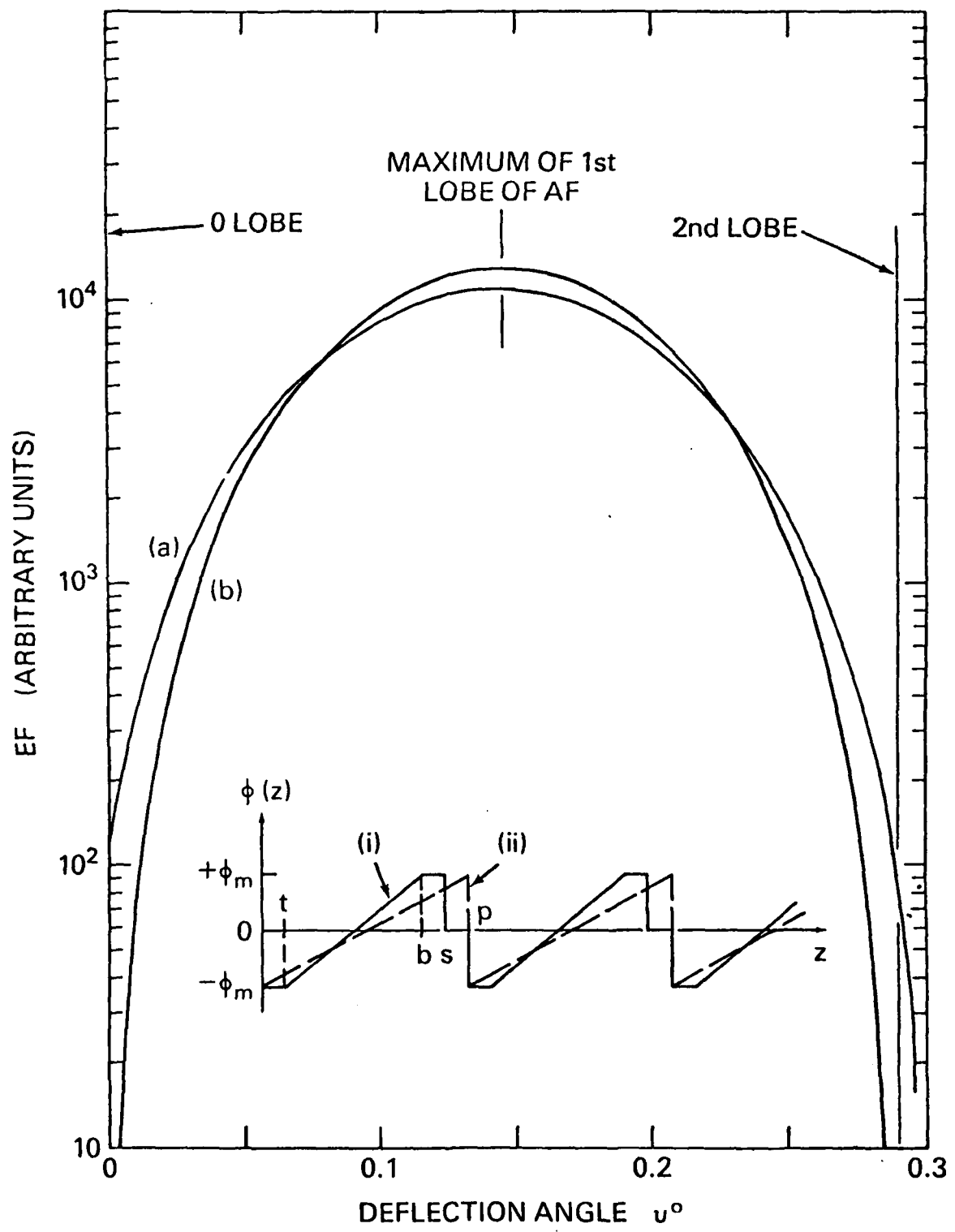


Fig. 12

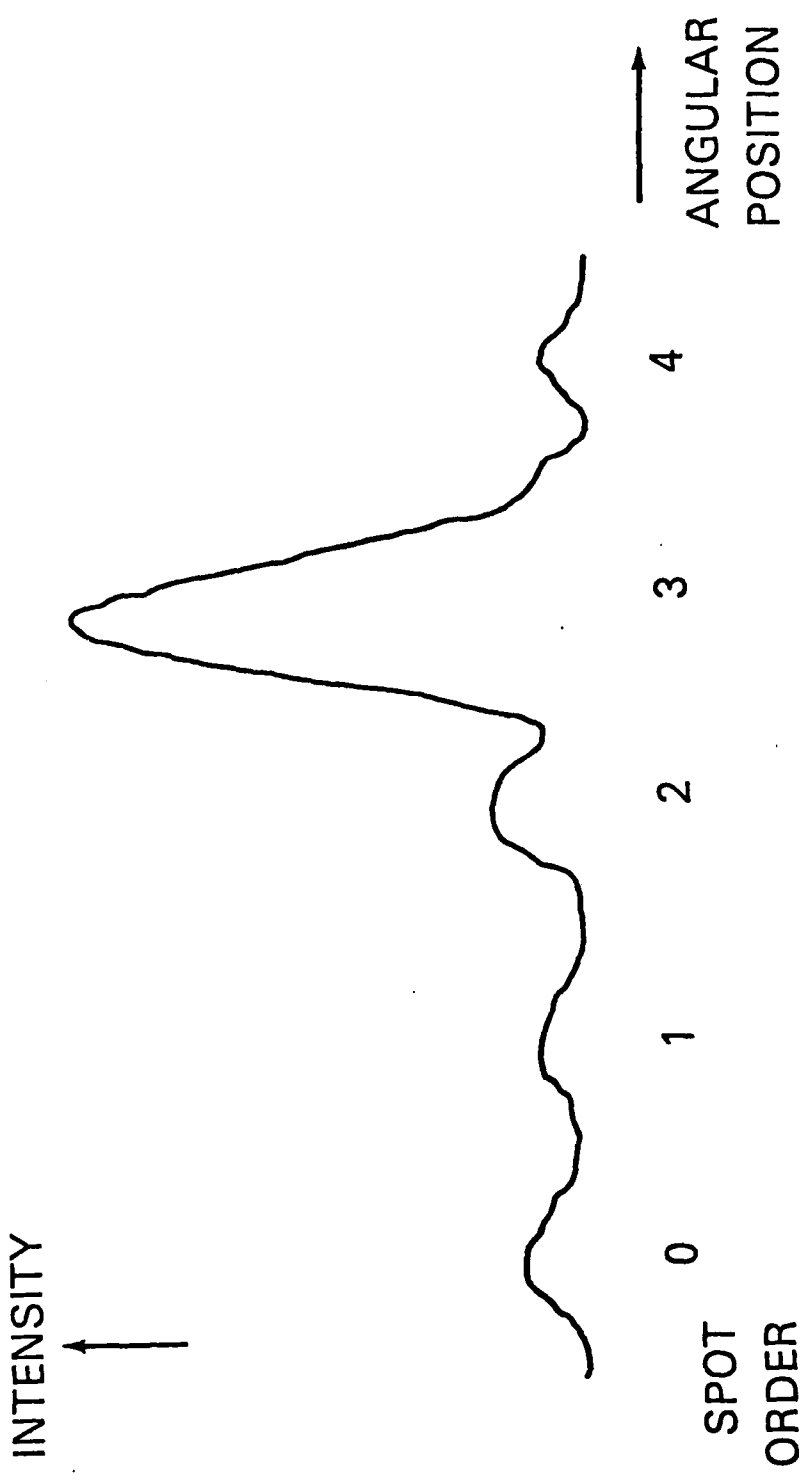


Fig. 13

**DATE
ILMED
-8**